




Cite this: *Nanoscale*, 2018, **10**, 9851

Received 1st April 2018,
Accepted 7th May 2018

DOI: 10.1039/c8nr02629g

rsc.li/nanoscale

Polymorphism of $\text{Ag}_{29}(\text{BDT})_{12}(\text{TPP})_4^{3-}$ cluster: interactions of secondary ligands and their effect on solid state luminescence†

Abhijit Nag,^a Papri Chakraborty,^a Mohammad Bodiuzzaman,^a Tripti Ahuja,^a Sudhadevi Antharjanam^b and Thalappil Pradeep *^a

We present the first example of polymorphism (cubic & trigonal) in single crystals of an atomically precise monolayer protected cluster, $\text{Ag}_{29}(\text{BDT})_{12}(\text{TPP})_4^{3-}$. We demonstrate that C–H... π interactions of the secondary ligands (TPP) are dominant in a cubic lattice compared to a trigonal lattice, resulting in a greater rigidity of the structure, which in turn, results in a higher luminescence efficiency in it.

Molecular species of noble metals often referred to as nanoclusters^{1–7} (NC) or aspicules^{8,9} have become an important research direction of advanced materials science. Some unprecedented structures and novel properties have been discovered, which enable new applications in catalysis, sensing, and optoelectronics.^{10–12} Ligand structures on metal surfaces and their non-covalent interactions drive self-organization of such systems leading to single crystals which may also be regarded as nanoparticle superlattices.^{13–16} While the primary ligands of a given cluster often protect the metal core, secondary ligands also contribute to the cluster stabilization for several of the emerging clusters.^{17–21} Therefore, intercluster interactions mediated through primary ligands or secondary ligands or a combination become possible, making different cluster assemblies. In the following, we describe the crystallization of two polymorphs of a well-known cluster,¹⁸ $\text{Ag}_{29}(\text{BDT})_{12}(\text{TPP})_4^{3-}$, by the dominant primary and secondary ligand interactions.

In the case of a well-known silver cluster,¹⁵ $\text{Ag}_{44}(\text{p-MBA})_{30}\text{Na}_4$, abbreviated as Ag_{44} , crystallization of the cluster occurs through hydrogen bonding (HB), a characteristic of carboxylic acid-bearing entities. The hexagonal network of HB resembles that of acid crystals such as terephthalic acid,²² tri-

mesic acid²³ and hexakis(4-carboxyphenyl)benzene.²⁴ As expected, protonation of the carboxylate groups on the cluster surface becomes a prerequisite of cluster formation. Similar non-covalent interactions can be observed in clusters such as Au_{102} ,¹⁴ Au_{246} ,¹³ Au_{103} ,¹⁶ etc. (the formulae are abbreviated), where primary interactions are HB, C–H... π and van der Waals (vdW) in nature, depending upon the ligands. These interactions, although weak, may have important electronic consequences such as luminescence. In this work, we explore the C–H... π and vdW interactions within the two polymorphs (cubic and trigonal) of the $[\text{Ag}_{29}(\text{BDT})_{12}(\text{TPP})_4]^{3-}$ cluster and their consequences in luminescence.

Bakr *et al.* reported the crystallization of $\text{Ag}_{29}(\text{BDT})_{12}(\text{TPP})_4^{3-}$ by slow evaporation of a dimethylformamide (DMF) solution of the cluster, drop cast on a microscope slide.¹⁸ More details of the crystallization processes are given in the ESI.† This method produced crystals which were packed in a cubic (C) lattice with a space group of $\text{Pa}\bar{3}$ (Fig. 1B). We changed the crystallization method of the NC to the vapor diffusion of methanol into a DMF solution of the clusters ($\sim 10 \text{ mg mL}^{-1}$). X-ray crystallographic analysis was performed at 296 K on the crystals obtained by this modified method. The crystal system was trigonal (T) (Fig. 1C) with the space group $\text{R}\bar{3}$ (Fig. 1D). So, $\text{Ag}_{29}(\text{BDT})_{12}(\text{TPP})_4^{3-}$ forms two polymorphs, T and C. Note that the color of the NCs of two polymorphs (orange for C and dark red for T) are visibly different under an optical microscope (Fig. S1†). The R_1 value for the C system is 8.94 but that of the T case is 7.68. The volume, density, and Z (number of molecules per unit cell) for this new T polymorph of the cluster are less compared to the previously reported C system (Fig. 1D). The reduced density of the T makes it possible to incorporate solvent molecules (DMF and methanol) in the unit cell.

The molecular structure of the NC is the same as that of the previously reported NC. The NC is composed of an Ag_{13} icosahedral core. Twelve silver atoms (green) cap all the 12 Ag atoms of the icosahedron, giving rise to four tetrahedrally oriented trigonal prisms (Fig. S2†). The remaining four Ag atoms (blue) face-cap the core at four tetrahedral positions.

^aDST Unit of Nanoscience (DST UNS) and Thematic Unit of Excellence, Department of Chemistry, Indian Institute of Technology Madras, Chennai 600036, India. E-mail: pradeep@iitm.ac.in; Fax: +91-44 2257-0545

^bSophisticated Analytical Instruments Facility (SAIF), Indian Institute of Technology Madras, Chennai 600036, India

† Electronic supplementary information (ESI) available. See DOI: 10.1039/c8nr02629g

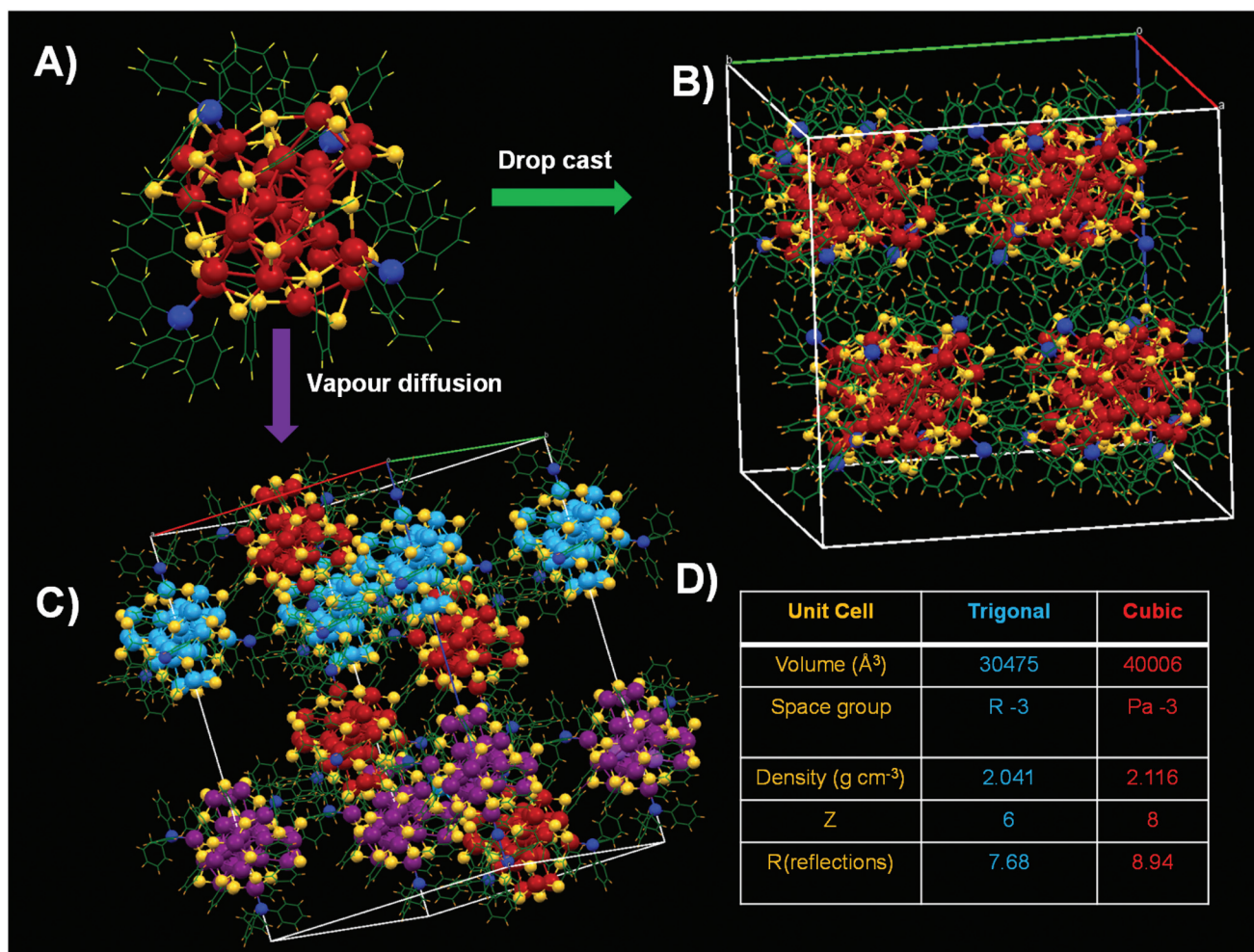


Fig. 1 (A) Crystal structure of $\text{Ag}_{29}(\text{BDT})_{12}(\text{TPP})_4^{3-}$. (B) Trigonal unit cell of the NC obtained by the vapour diffusion method. (C) Cubic unit cell of the NC obtained by the drop casting method. (D) Comparison of the unit cell parameters for both the polymorphs.

The four TPP (phosphorus as pink) ligands are connected with the tetrahedrally oriented four silver atoms (Fig. S2†).

One S moiety of the BDT ligand is attached to each of the 12 Ag atoms of the icosahedron and the remaining S moieties bridge Ag atoms of each Ag_3S_6 crown. The total number of S atoms is 24 $\{(24 = 12 \text{ S atoms attach to the 12 Ag icosahedron core} + 4) \times (\text{Ag}_3\text{S}_6 \text{ crown motif})\}$.

For the T system, in the (001) plane (view from the Z-axis) of the crystal lattice, the NCs get organized into a hexagonal lattice with a 3-fold axis passing through the center of the molecule (Fig. 2A), while for the (100) (view from the X-axis) (Fig. 2B) and (010) (view from the Y-axis) (Fig. 2C) planes, the NCs get decorated into a rectangular lattice. Viewing from the Z axis, the NCs form two different parallel (001) and (00-1) planes. Each NC from the two (001) and (00-1) planes has a center of inversion (Fig. 2D). The interparticle distance of 1.79 nm (less than the 2.74 nm overall size of the NCs) arises from ligand interlocking. For the C system, the NCs assemble into a simple square lattice in the (001) plane (view from the Z axis). The interparticle distance is 1.75 nm, less than the

overall size 2.74 nm of the nanocrystal. In the case of Au_{246} , the interparticle distance was of 3.1 nm, less than the 3.3 nm overall size of the NC.¹³

When zooming into the surfaces of the NCs, the T and C packing are related to the alignment of their surface ligands. The BDT (primary) and TPP (secondary) ligands are highly ordered and are self-assembled on the silver surface (Fig. S3–5 & S7, 8†).

For the T system, the BDT ligands of the two NCs formed cyclohexane chair patterns in the unit cell. C–H $\cdots\pi$ and H \cdots H vdW are the interactions present to form such types of cyclohexane chair structures (Fig. 3A). For a NC, there will be a maximum of four such types of interactions in a T unit cell. The C–H $\cdots\pi$ and H \cdots H distances were ~ 2.82 and ~ 2.36 Å, respectively. In the C system, every NC has the same six types of interactions with slight changes in the distances.

For BDT and TPP ligands, there are two types of interactions: (i) intra-cluster interactions and (ii) inter-cluster interactions.

(i) The C–H groups of the TPP ligands (red) interact with the benzene ring of the BDT ligands in intra-cluster inter-

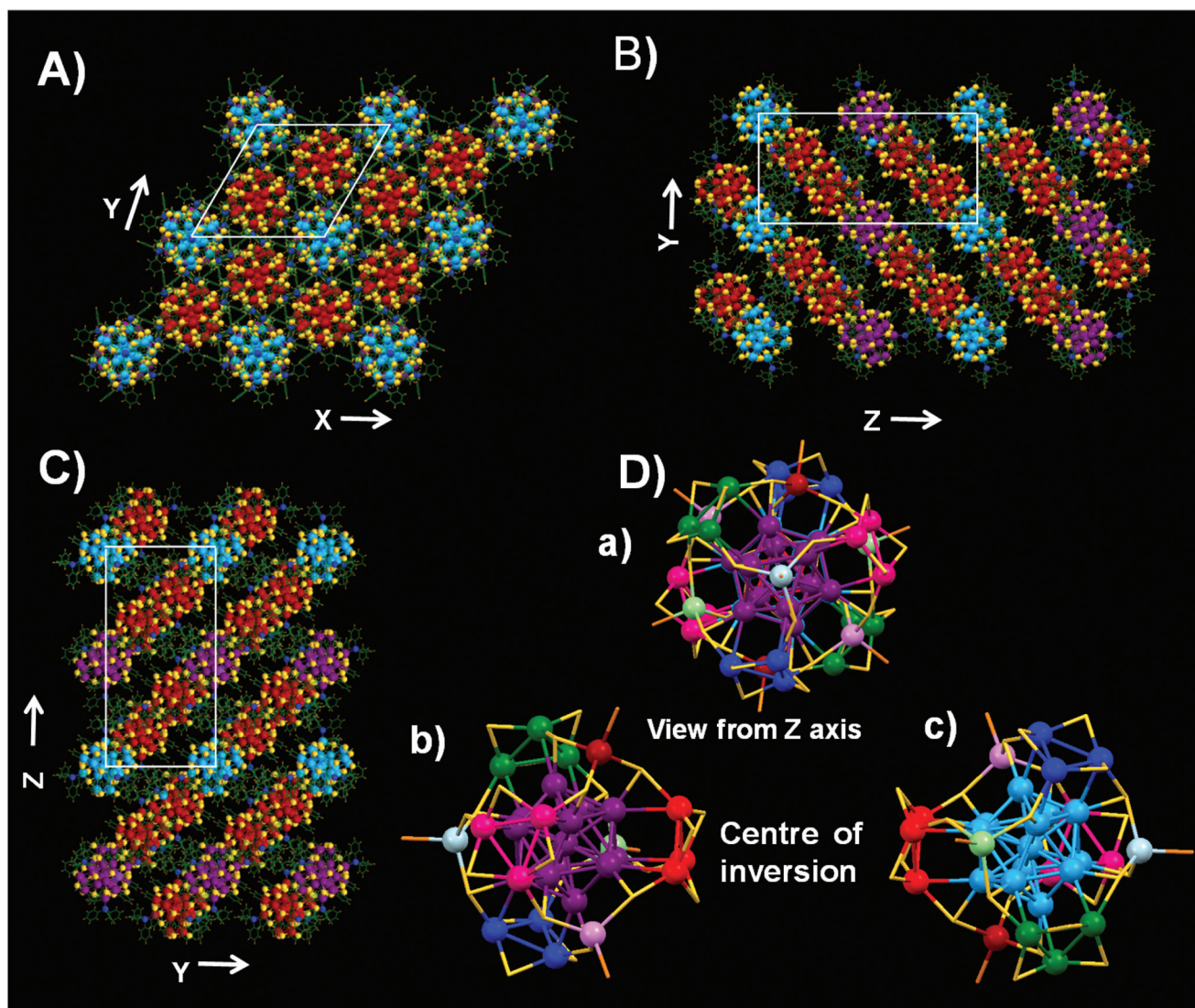


Fig. 2 Packing of the crystal view from the (A) Z-axis, (B) Y-axis and (C) X-axis. (D) (a) View of the cluster packing from the Z-axis. Two NCs formed two different (001) and (00-1) layered planes; (b) and (c) are the two different clusters of (a). They have a center of inversion.

actions (Fig. 3B & S5A†). For C and T systems, the interactions are similar with small changes in interaction distances. Here, C-H... π interaction distances are ~ 2.77 and 2.92 Å for the C and the T systems, respectively. The orientations of the benzene rings of the TPP are controlled by these C-H... π interactions. The TPP ligands fit into the cavity formed by the BDT ligands by these types of interactions (Fig. 3B).

(ii) The C-H groups of the BDT (orange) interact with the benzene ring of the TPP leading to inter-cluster interactions (Fig. 3C & S5B†). Here also, the interactions are similar with slight changes in interaction distances for both types of unit cells. The C-H... π interaction distances are ~ 3.07 – 3.39 Å and 2.92 Å for the C and the T systems, respectively.

T-shaped C-H... π interactions are present between the TPP ligands in the C unit cell (Fig. 4A). In a unit cell, eight TPP ligands, by interlocking each other, form a hexagonal shape

through C-H... π interactions from the eight NCs (Fig. 4A). The average C-H... π distance was ~ 2.88 Å. Strong C-H... π interactions of the TPP ligands form a polymeric chain to hold each NC (Fig. S7A†). Every NC is directly or indirectly connected with the other NCs by C-H... π interactions of the TPP ligands. This distance is consistent with the reported value for typical C-H... π interactions in the Au₂₄₆ NCs¹³ with -SPh-*p*-CH₃ ligands (2.88 ± 0.42 Å) but somewhat larger than the C-H... π distance in the Au₁₀₃ NCs¹⁶ composed of -S-Nap ligands (2.76 ± 0.05 Å). In the T system, the C-H... π interaction distances for TPP ligands were in the range of ~ 3.12 – 3.37 Å (Fig. S8D†). Here, the interaction energy is less compared to C as the distance is larger. There are breakages in C-H... π interactions for TPP ligands (Fig. S8B & C†). Such orientations and self-organized surface patterns of ligands are reminiscent of the α -helix²⁵ and β -sheet in proteins, and also in the recently

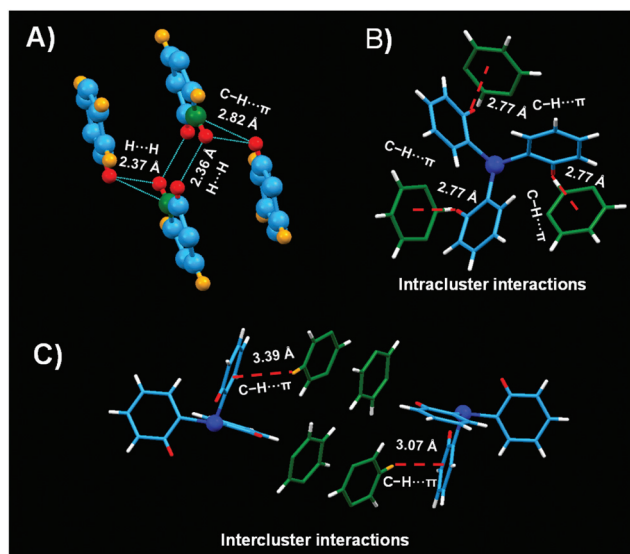


Fig. 3 (A) Interactions among the BDT ligands from two different NCs in the trigonal structure. The BDT ligands of the two NCs formed cyclohexane chair patterns in the unit cell. (B) Intra-cluster interactions between C–H of the TPP with the benzene ring of BDT in the cubic system. (C) Inter-cluster interactions between C–H of the BDT with the benzene ring of the TPP in the cubic system.

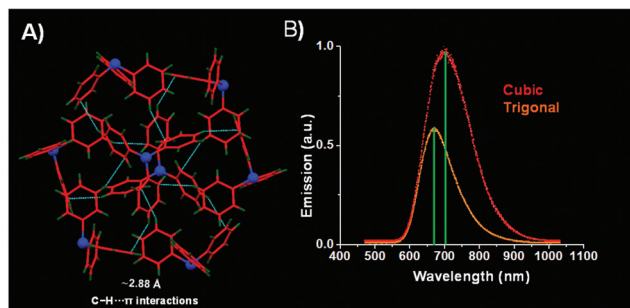


Fig. 4 (A) C–H... π interactions of the TPP ligands in the cubic system. (B) Emission spectra of the single crystals for both the cubic and the trigonal systems.

reported Au₂₄₆¹³ and Au₁₀₃¹⁶ NCs. So, NCs could exhibit a level of structural complexity comparable to that of biomolecules.

The secondary structures of proteins are mainly stabilized by hydrogen bonds.²⁶ Here, the surface patterns on the NCs are stabilized by intermolecular C–H... π and vdW interactions.

We note that the surface patterns and orientations are induced by specific crystallization because the C–H... π interactions are different for different crystal systems of the same NC.

The emission spectra of both NCs, collected at room temperature, are shown in Fig. 4B. Both the NCs can be efficiently excited at $\lambda_{\text{max}} = 532$ nm. Upon comparing both the NCs, two main features were observed:

(i) The cubic NCs are more luminescent than the trigonal NCs: Inter C–H... π interactions for secondary ligands (TPP) are more facilitated in C than in T (Fig. S7 & 8†). As a result, the C lattice becomes more rigid compared to the T lattice. Greater rigidity, in turn, results in a higher luminescence efficiency for the C system.²⁷ The C–H... π interactions significantly restrict the intramolecular rotations and vibrations and thus enhance the radiative transitions considerably in the crystalline state.²⁸ Secondary ligands play a crucial role to increase the luminescence efficiency of the NCs.

(ii) A red shift of the emission band occurs for the cubic NCs by more than 30 nm: The red shift can be explained in terms of electronic coupling between the NCs *via* interactions between the transition dipole moments of the individual Ag₂₉(BDT)₁₂(TPP)₄ NCs and the induced dipole moments in the neighboring Ag₂₉(BDT)₁₂(TPP)₄ NCs in the single crystal. This interaction is expected to lower the transition energy.^{29,30} The red shift of the emission band is expected to be caused by a combined effect of the electronic coupling and the non-radiative decay pathways occurring through electron–phonon interactions that lower the emission energy.¹⁸

Conclusions

In summary, we demonstrate that polymorphism exists in atomically precise cluster systems. The packing of [Ag₂₉(BDT)₁₂(TPP)₄]^{3–} clusters into two different polymorphic forms, cubic and trigonal, was favored by different patterns of intercluster and intracluster interactions. The greater extent of C–H... π interactions in the cubic NCs makes them more rigid and hence more luminescent than the trigonal NCs. This also highlights the role of secondary ligands in enhancing the luminescence properties of the clusters. The discovery of polymorphism in atomically precise clusters opens up a new dimension in nanoparticle engineering, presenting the possibility of engineering NC unit cells with enhanced optical, mechanical and electrical properties.

Conflicts of interest

There are no conflicts to declare.

Acknowledgements

We acknowledge the Department of Science and Technology, Government of India for constantly supporting our research program on nanomaterials. A. N. and T. A. thank IIT Madras for doctoral fellowships. P. C. thanks the Council of Scientific and Industrial Research (CSIR) for her research fellowship. M. B. thanks the University Grants Commission (UGC) for his research fellowship.

References

- 1 I. Chakraborty and T. Pradeep, *Chem. Rev.*, 2017, **117**, 8208–8271.
- 2 R. Jin, C. Zeng, M. Zhou and Y. Chen, *Chem. Rev.*, 2016, **116**, 10346–10413.
- 3 M. Zhu, C. M. Aikens, F. J. Hollander, G. C. Schatz and R. Jin, *J. Am. Chem. Soc.*, 2008, **130**, 5883–5885.
- 4 M. W. Heaven, A. Dass, P. S. White, K. M. Holt and R. W. Murray, *J. Am. Chem. Soc.*, 2008, **130**, 3754–3755.
- 5 C. P. Joshi, M. S. Bootharaju, M. J. Alhilaly and O. M. Bakr, *J. Am. Chem. Soc.*, 2015, **137**, 11578–11581.
- 6 H. Qian, W. T. Eckenhoff, Y. Zhu, T. Pintauer and R. Jin, *J. Am. Chem. Soc.*, 2010, **132**, 8280–8281.
- 7 N. A. Sakthivel, S. Theivendran, V. Ganeshraj, A. G. Oliver and A. Dass, *J. Am. Chem. Soc.*, 2017, **139**, 15450–15459.
- 8 G. Natarajan, A. Mathew, Y. Negishi, R. L. Whetten and T. Pradeep, *J. Phys. Chem. C*, 2015, **119**, 27768–27785.
- 9 K. R. Krishnadas, A. Baksi, A. Ghosh, G. Natarajan, A. Som and T. Pradeep, *Acc. Chem. Res.*, 2017, **50**, 1988–1996.
- 10 G. Li and R. Jin, *Acc. Chem. Res.*, 2013, **46**, 1749–1758.
- 11 S. Yamazoe, T. Yoskamtorn, S. Takano, S. Yadnum, J. Limtrakul and T. Tsukuda, *Chem. Rec.*, 2016, **16**, 2338–2348.
- 12 W. W. Xu, B. Zhu, X. C. Zeng and Y. Gao, *Nat. Commun.*, 2016, **7**, 13574.
- 13 C. Zeng, Y. Chen, K. Kirschbaum, K. J. Lambright and R. Jin, *Science*, 2016, **354**, 1580–1584.
- 14 P. D. Jadzinsky, G. Calero, C. J. Ackerson, D. A. Bushnell and R. D. Kornberg, *Science*, 2007, **318**, 430–433.
- 15 B. Yoon, W. D. Luedtke, R. N. Barnett, J. Gao, A. Desireddy, B. E. Conn, T. Bigioni and U. Landman, *Nat. Mater.*, 2014, **13**, 807.
- 16 T. Higaki, C. Liu, M. Zhou, T.-Y. Luo, N. L. Rosi and R. Jin, *J. Am. Chem. Soc.*, 2017, **139**, 9994–10001.
- 17 M. J. Alhilaly, M. S. Bootharaju, C. P. Joshi, T. M. Besong, A.-H. Emwas, R. Juarez-Mosqueda, S. Kaappa, S. Malola, K. Adil, A. Shkurenko, H. Häkkinen, M. Eddaoudi and O. M. Bakr, *J. Am. Chem. Soc.*, 2016, **138**, 14727–14732.
- 18 L. G. AbdulHalim, M. S. Bootharaju, Q. Tang, S. Del Gobbo, R. G. AbdulHalim, M. Eddaoudi, D.-e. Jiang and O. M. Bakr, *J. Am. Chem. Soc.*, 2015, **137**, 11970–11975.
- 19 M. S. Bootharaju, R. Dey, L. E. Gevers, M. N. Hedhili, J.-M. Basset and O. M. Bakr, *J. Am. Chem. Soc.*, 2016, **138**, 13770–13773.
- 20 P. Chakraborty, A. Nag, G. Paramasivam, G. Natarajan and T. Pradeep, *ACS Nano*, 2018, **12**, 2415–2425.
- 21 A. Ghosh, M. Bodiuzzaman, A. Nag, M. Jash, A. Baksi and T. Pradeep, *ACS Nano*, 2017, **11**, 11145–11151.
- 22 M. C. Etter, *Acc. Chem. Res.*, 1990, **23**, 120–126.
- 23 S. V. Kolotuchin, E. E. Fenlon, S. R. Wilson, C. J. Loweth and S. C. Zimmerman, *Angew. Chem., Int. Ed. Engl.*, 1996, **34**, 2654–2657.
- 24 K. Kobayashi, T. Shirasaka, E. Horn and N. Furukawa, *Tetrahedron Lett.*, 2000, **41**, 89–93.
- 25 J. D. Dunitz, *Angew. Chem., Int. Ed.*, 2001, **40**, 4167–4173.
- 26 L. Pauling, R. B. Corey and H. R. Branson, *Proc. Natl. Acad. Sci. U. S. A.*, 1951, **37**, 205–211.
- 27 K. A. Denault, J. Brgoch, M. W. Gaultois, A. Mikhailovsky, R. Petry, H. Winkler, S. P. DenBaars and R. Seshadri, *Chem. Mater.*, 2014, **26**, 2275–2282.
- 28 T. Chen, S. Yang, J. Chai, Y. Song, J. Fan, B. Rao, H. Sheng, H. Yu and M. Zhu, *Sci. Adv.*, 2017, **3**, e1700956.
- 29 H. Döllefeld, H. Weller and A. Eychmüller, *J. Phys. Chem. B*, 2002, **106**, 5604–5608.
- 30 J. Zhang, C. Rowland, Y. Liu, H. Xiong, S. Kwon, E. Shevchenko, R. D. Schaller, V. B. Prakapenka, S. Tkachev and T. Rajh, *J. Am. Chem. Soc.*, 2015, **137**, 742–749.